# Thermal Reactions of Benzoxazole. Single Pulse Shock Tube Experiments and Quantum Chemical Calculations

**Assa Lifshitz,* Carmen Tamburu, Aya Suslensky, and Faina Dubnikova**

*Department of Physical Chemistry, The Hebrew University, Jerusalem 91904, Israel*

*Received: December 5, 2005; In Final Form: January 29, 2006*

The thermal decomposition of benzoxazole diluted in argon was studied behind reflected shock waves in a 2 in. i.d. single-pulse shock tube over the temperature range 1000−1350 K and at overall densities of $\sim 3 \times 10^{-5}$ mol/cm$^3$. Two major products, *o*-hydroxybenzonitrile at high concentration and cyclopentadiene carbonitrile (accompanied by carbon monoxide) at much lower concentration, and four minor fragmentation products resulting from the decomposition were found in the postshock samples. They were, in order of decreasing abundance, benzonitrile, acetylene, HCN, and CH═C−CN and comprised of only a few percent of the overall product distribution. Quantum chemical calculations were carried out to determine the sequence of the unimolecular reactions that led to the formation of *o*-hydroxybenzonitrile and cyclopentadiene carbonitrile, the major products of the thermal reactions of benzoxazole. A potential energy surface leading directly from benzoxazole to cyclopentadiene carbonitrile could not be found, and it was shown that the latter is formed from the product *o*-hydroxybenzonitrile. In order that cyclopentadiene carbonitrile be produced, CO elimination and ring contraction from a six- to a five-membered ring must take place. A surface where CO elimination occurs prior to ring contraction was found to have very high barriers compared to the ones where ring contraction occurs prior to CO elimination and was not considered in our discussion. Rates for all the steps on the various surfaces were evaluated, kinetic schemes containing these steps were constructed, and multiwell calculations were performed to evaluate the mole percent of the two major products as a function of temperature. The agreement between the experimental results and these calculations, as shown graphically, is very good.

## I. Introduction

Benzoxazole is a five-membered ring compound containing both nitrogen and oxygen fused to a benzene ring. It differs from its two isomers 1,2-benzisoxazole and 2,1-benzisoxazole in the location of the nitrogen relative to the carbon/oxygen atoms in the five-membered oxazole ring.

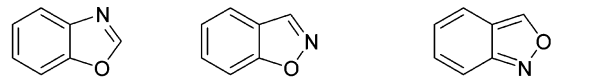

benzoxazole 1,2-benzisoxazole 2,1-benzisoxazole (anthranil)

Benzoxazole does not have a weak N−O bond and contains a resonance-stabilized benzene ring. It is thus more stable and is expected to start decomposing at a temperature higher than those of its two benzisoxazole isomers under the same conditions. The heats of formation of these three isomers are 10.8 kcal/mol for benzoxazole,[1] 33.3 kcal/mol for 1,2-benzisoxazole,[2] and 41.2 kcal/mol for 2,1-benzisoxazole[2] (anthranil) at 298.15 K.

We have recently published[3] a detailed investigation on the thermal decomposition and isomerization of 2,1-benzisoxazole both experimentally and by quantum chemical calculations over the temperature range 825−1000 K. It was shown that, in addition to very minute fragmentation, 2,1-benzisoxazole undergoes two main reactions: (1) ring contraction with the formation of cyclopentadienecarbonitrile and carbon monoxide and (2) formation of phenylnitrene, which was identified by its formation of aniline upon absorption of two hydrogen atoms.

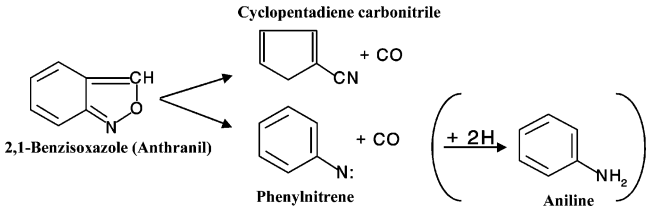


It did not isomerize to *o*-hydroxybenzonitrile, as the distance between the oxygen atom and the six-membered ring does not allow such an isomerization process to take place.

We are not aware of previous studies on the homogeneous decomposition of benzoxazole. In this paper we present experimental shock tube results and quantum chemical calculations on the isomerization and the CO elimination from benzoxazole to form *o*-hydroxybenzonitrile and cyclopentadienecarbonitrile.

## II. Experimental Section

**1. Shock Tube, Materials and Analysis.** The thermal decomposition of benzoxazole was studied behind reflected shock waves in a pressurized driver, 2 in. i.d. single pulse shock tube. The driven section was 4 m long and the driver had a variable length up to a maximum of 2.7 m and could be varied in small steps in order to tune for the best cooling conditions. A 36-L dump tank was connected to the driven section near

* Corresponding author. Office: 972-2-658 5865. Fax: 972-2-561 7812. E-mail: Assa@vms.huji.ac.il.

10.1021/jp057063u CCC: $33.50 
Published on Web 03/11/2006

the diaphragm holder in order to quench transmitted shocks. The tube, the gas handling system, the reaction mixture bulbs, and the transfer tubes were all maintained at 170 °C with an accuracy of ±2 °C. The shock tube and the mode of its operation were described in the past.[4]

Reflected shock temperatures were determined from the extent of decomposition of 1,1,1-trifluoroethane ($CH_3CF_3$) that was added in small quantities to the reaction mixtures to serve as an internal standard. Its decomposition to $CH_2{=}CF_2 + HF$ is a first-order unimolecular reaction that under the temperature and pressure of this investigation has a rate constant of $k_{first} = 10^{14.85} \exp(-74.05 \times 10^3/RT)\ s^{-1}$, where $R$ is expressed in units of cal/(K mol).[5] Reflected shock temperatures were then calculated from the relation

$$T = -(E/R)/\left[\ln\left\{-\frac{1}{At}\ln(1-\chi)\right\}\right]$$

where $t$ is the reaction dwell time, approximately 2 ms, $A$ and $E$ are the Arrhenius parameters of the standard reaction, and $\chi$ is the extent of decomposition defined as

$$\chi = [CH_2{=}CF_2]_t/([CH_2{=}CF_2]_t + [CH_3CF_3]_t)$$

Density ratios were calculated from the measured incident shock velocities using the three conservation equations and the ideal gas equation of state. Total densities behind the reflected shock, $C_5$, in all the experiments were around $3 \times 10^{-5}$ mol/cm$^3$. Cooling rates were approximately $5 \times 10^5$ K/s.

After pumping down a 12-L glass bulb to $\sim 10^{-5}$ Torr, an amount of liquid corresponding to 0.5% benzoxazole was injected into the evacuated bulb that was then filled to 1 atm with argon containing 0.08% of the internal standard, $CH_3CF_3$. The bulb served as storage for the reaction mixture.

Two gas chromatographic analyses for each postshock mixture provided the product distribution and the temperature. A flame ionization detector (FID) with a 2-m temperature-programmed Porapak N column was used to determine the ratio $[CH_2{=}CF_2]_t/([CH_2{=}CF_2]_t + [CH_3CF_3])$ for the temperature calculation. A nitrogen phosphorus detector (NPD) with a 2-m temperature-programmed Tenax column was used to determine the nitrogen-containing species. The concentration of carbon monoxide was evaluated from nitrogen−oxygen mass balance considerations assuming that there was a minimal loss of material if at all. A typical chromatogram showing traces obtained on the two detectors is given in Figure 1.

**2. Experimental Results.** To determine the distribution of reaction products, some 60 tests were run, covering the temperature range 1000−1350 K. Figure 2 shows the general product distribution over the entire temperature range. As can be seen, *o*-hydroxybenzonitrile is of the highest concentration, followed by cyclopentadiene carbonitrile and carbon monoxide (that is formed in parallel), and at lower concentrations are the four fragmentation products benzonitrile, acetylene, hydrogen cyanide, and cyanoacetylene. Figure 3 shows the experimental mole percent for each one of the products.

## III. Computational Details

**1. Quantum Chemical Calculations**. We used the Becke three-parameter hybrid method[6] with Lee−Yang−Parr correlation functional approximation (B3LYP)[7] and the Dunning correlation consistent polarized valence double $\xi$ (cc-pVDZ) basis set.[8] Structure optimization of the reactants and products was done using the Berny geometry optimization algorithm.[9] For determining transition state structures, we used the combined

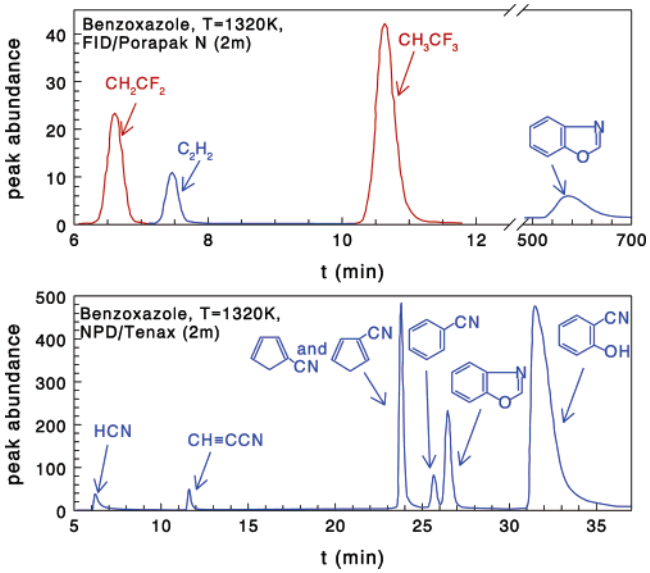


**Figure 1.** A gas chromatograph showing the products of benzoxazole decomposition. Top: $CH_3CF_3$ and $CH_2{=}CF_2$, from the ratio of which the temperature behind the reflected shock is calculated. Bottom: NPD spectrum of the fragmentation products.

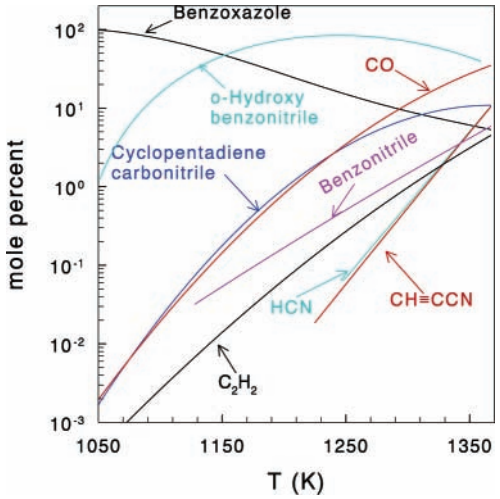


**Figure 2.** General distribution of the reaction products in the decomposition of benzoxazole.

synchronous transit-guided quasi-Newton (STQN) method.[10] The higher level calculations were done using these geometries.

All the calculations were performed on singlet surfaces without symmetry restrictions**.** Vibrational analyses were done at the same level of theory to characterize the optimized structures as local minima or transition states. Calculated vibrational frequencies and entropies (at the B3LYP level) were used to evaluate pre-exponential factors of the reactions under consideration. All the calculated frequencies, the zero point energies, and the thermal energies are of harmonic oscillators. The calculations of the intrinsic reaction coordinate (IRC), to check whether the transition states under consideration connect the expected reactants and products, were done at the B3LYP level of theory with the same basis set as was used for the stationary point optimization**.** These calculations were done on all the transition states.

Each optimized B3LYP structure was recalculated at a single-point quadratic CI including single and double substitutions with a triple contribution to the energy−QCISD(T).[11] All of the reported relative energies include zero-point energy (ZPE) correction.

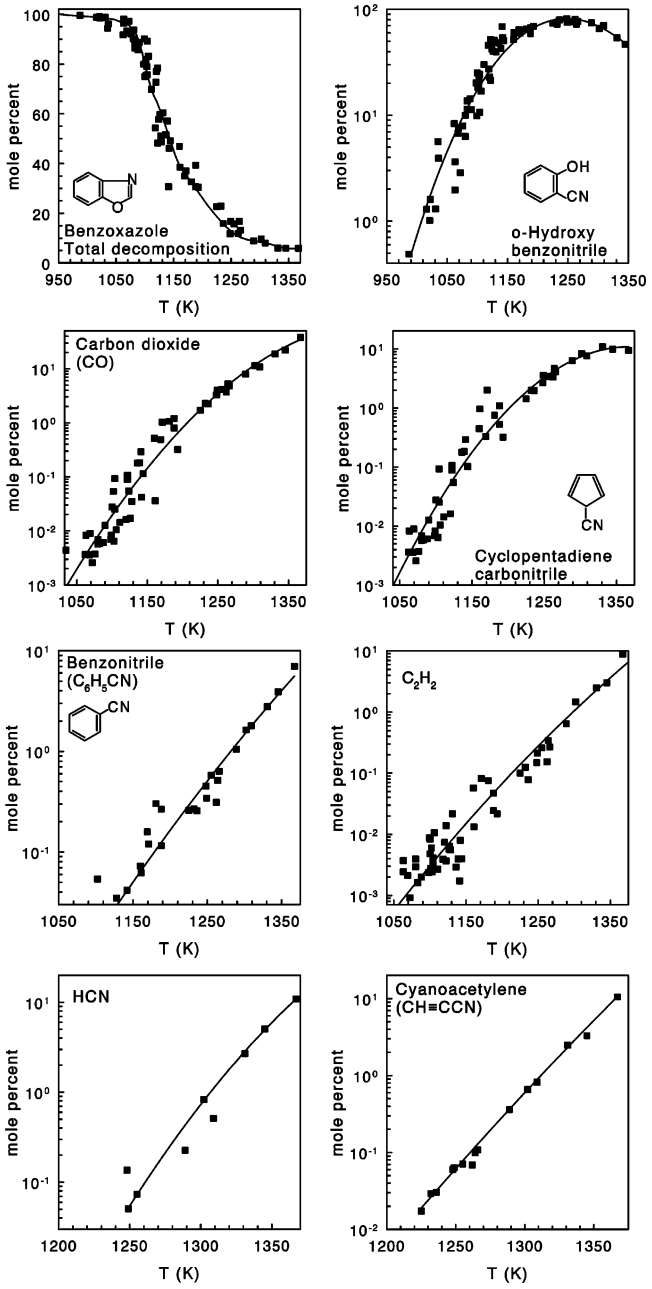


**Figure 3.** A detailed distribution of the reaction products in the decomposition of benzoxazole.

The DFT and QCISD(T) computations were carried out using the Gaussian 98 program package[12] and were done on a DEC Alpha XP1000 1/667 professional workstation.

**2. Rate Constant Calculations.** To evaluate the high-pressure-limit first-order rate constants from the quantum chemical calculations, the relation

$$k_\infty = \Gamma(T)\sigma\,(kT/h)\,\exp(\Delta S^{\ddagger}/R)\,\exp(-\Delta H^{\ddagger}/RT)$$

was used,[13,14] where $h$ is Planck's constant, $k$ is the Boltzmann factor, $\sigma$ is the degeneracy of the reaction coordinate (one in all the calculations), $\Delta H^{\ddagger}$ and $\Delta S^{\ddagger}$ are the temperature dependent enthalpy and entropy of activation, respectively, and $\Gamma(T)$ is the tunneling correction. Since we deal with unimolecular reactions, $\Delta H^{\ddagger} = \Delta E^{\ddagger}$, where $\Delta E^{\ddagger}$ is the energy difference between the transition state and the reactant. $\Delta E^{\ddagger}$ is equal to $\Delta E^{0}_{\text{total}} + \Delta E_{\text{thermal}}$, where $\Delta E^{0}_{\text{total}}$ is obtained by taking the difference between the total energies of the transition state and the reactant and $\Delta E_{\text{thermal}}$ is the difference between the thermal energies of these species.

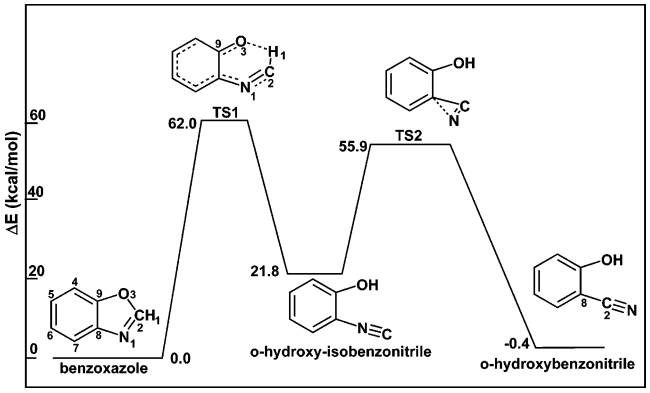


**Figure 4.** Reaction pathway of benzoxazole isomerization. Relative energies (in kcal/mol) are calculated at the uQCISD(T)//uB3LYP/cc-pVDZ level of theory.

The tunneling effect, $\Gamma(T)$, was estimated using Wigner's inverted harmonic model,[15] where

$$\Gamma(T) = 1 + \frac{1}{24} \times \left(\frac{hc\nu}{kT}\right)^2$$

and $\nu$ is the imaginary frequency of the reaction coordinate in $cm^{-1}$.[16,17]

## IV. Results of the Quantum Chemical Calculations

**1. Formation of *o*-Hydroxybenzonitrile.** The potential energy surface of benzoxazole → *o*-hydroxybenzonitrile isomerization is shown in Figure 4 with the atom numbering. The energetics and other parameters relevant to this surface are shown in Table 1. Selected structural parameters of the species on the surface are shown in Table 2.

The surface contains two transition states and one intermediate. The first step is C(2)−O(3) bond breaking together with 1,5-H-atom migration from C(2) to O(3) in what used to be the five-membered ring. The C(2)−H(1) bond in the transition state TS1 becomes longer (1.130 Å compared to 1.088 Å in the reactant) and atoms O(3) and H(1) come closer, to a distance of 1.612 Å as compared to 2.087 Å, in the reactant, toward the formation of the O(3)−H(1) bond. The C(2)−O(3) bond breaking results in the formation of a C(9)═O(3) double bond instead of a single bond in benzoxazole. This process is accompanied by some loss of resonance in the benzene ring that is later restored in the formation of *o*-hydroxyisobenzonitrile. The energy level of the transition state TS1 is 62 kcal/mol at the QCISD(T)//B3LYP/cc-pVDZ level of theory and it is the highest energy level on the surface. The second step is the isomerization from *o*-hydroxyisobenzonitrile to *o*-hydroxybenzonitrile with a barrier of ∼34 kcal/mol. This barrier is very similar to the barrier in the same process with a $CH_3$ group (instead of OH), which is 35.2 kcal/mol.[18]

It is interesting to note, as can be seen in Figure 2, that the concentration of *o*-hydroxybenzonitrile exceeds that of benzoxazole already at 1150 K, although the heat of formation of these two compounds are practically identical. The driving force for this isomerization is the relatively large entropy change (∼7 cal/mol, Table 1) in the process. This entropy change means that the back reaction of the isomerization would be considerably slower than the forward reaction.

*o*-Hydroxybenzonitrile is the main product in the postshock mixture of heated benzoxazole. There is, however, an additional

**TABLE 1: Total Energies $E_{total}$ (in au), Zero Point Energies, Relative Energies $\Delta E$,[a] Imaginary Frequencies,[b] and Entropies[c] of the Species on the Benzoxazole → *o*-Hydroxybenzonitrile Potential Energy Surface**

| | B3LYP | | | | | QCISD(T) | |
|---|---|---|---|---|---|---|---|
| species | $E_{total}$ | $\Delta E^a$ | ZPE | $S^c$ | $\nu^b$ | $E_{total}$ | $\Delta E^a$ |
| benzoxazole | −399.749615 | 0.0 | 66.4 | 77.32 | | −398.657612 | 0.0 |
| TS1 | −399.647214 | 59.2 | 61.3 | 82.46 | (i − 1011) | −398.550788 | 62.0 |
| *o*-hydroxyisobenzonitrile | −399.708132 | 24.1 | 64.4 | 84.07 | | −398.619664 | 21.8 |
| TS2 | −399.649200 | 59.9 | 63.0 | 83.58 | (i − 400) | −398.562992 | 55.9 |
| *o*-hydroxybenzonitrile | −399.742953 | 2.7 | 64.9 | 83.57 | | −398.655963 | −0.4 |

[a] Relative energies in kcal/mol. $\Delta E = \Delta E_{total} + \Delta(ZPE)$. [b] Imaginary frequency in $cm^{-1}$ [c] Entropies at 298 K in cal/(K mol).

**TABLE 2: Several Structural Parameters of the Species Involved in the Reaction Benzoxazole → *o*-Hydroxybenzonitrile Calculated at the B3LYP/cc-pVDZ Level of Theory**

| parameter[a,b] | benzoxazole | TS1 | *o*-hydroxy-isobenzonitrile | TS2 | *o*-hydroxy-benzonitrile |
|---|---|---|---|---|---|
| N(1)−C(2) | 1.291 | 1.194 | 1.184 | 1.202 | 1.166 |
| C(2)−O(3) | 1.372 | 2.119 | 3.347 | – | – |
| O(3)−C(9) | 1.374 | 1.294 | 1.353 | 1.349 | 1.353 |
| C(9)−C(4) | 1.390 | 1.424 | 1.400 | 1.402 | 1.401 |
| C(4)−C(5) | 1.398 | 1.389 | 1.394 | 1.394 | 1.392 |
| C(5)−C(6) | 1.410 | 1.408 | 1.402 | 1.403 | 1.403 |
| C(6)−C(7) | 1.396 | 1.390 | 1.392 | 1.392 | 1.390 |
| C(7)−C(8) | 1.400 | 1.395 | 1.402 | 1.401 | 1.415 |
| C(8)−C(9) | 1.403 | 1.444 | 1.412 | 1.410 | 1.415 |
| C(8)−N(1) | 1.401 | 1.406 | 1.398 | 1.861 | – |
| C(2)−H(1) | 1.088 | 1.130 | 2.696 | – | – |
| O(3)−H(1) | 2.087 | 1.612 | 0.972 | 0.973 | 0.973 |
| C(2)−C(8) | – | – | 2.572 | 1.619 | 1.432 |

[a] Distances are in angstroms. [b] The atom numbering is shown in Figure 4.

product, cyclopentadienecarbonitrile. It is a main product, although its concentration is considerably lower than that of *o*-hydroxybenzonitrile.

**2. Formation of Cyclopentadienecarbonitrile.** We searched for a potential energy surface that would lead directly from benzoxazole to cyclopentadienecarbonitrile. Despite many efforts, we could not find such a surface. We therefore concluded that cyclopentadienecarbonitrile is formed from *o*-hydroxybenzonitrile rather than directly from benzoxazole. This conclusion was also supported, to some extent, by the fact that the concentration of cyclopentadienecarbonitrile was much lower than that of *o*-hydroxybenzonitrile.

Two potential energy surfaces for the formation of cyclopentadienecarbonitrile from *o*-hydroxybenzonitrile that were found are shown in Figures 5 and 6 with the atom numbering. The difference between the two surfaces is that one leads to the formation of 1,3-cyclopentadiene-1-carbonitrile as the final product (Figure 5) and the second one to 1,3-cyclopentadiene-2-carbonitrile as the final product (Figure 6). There are also some differences in the exact pathways. The energetics and other parameters relevant to these surfaces are shown in Table 3. Selected structural parameters of the species on the surfaces are shown in Tables 4 and 5.

In order that cyclopentadienecarbonitrile be formed, both contraction of the six- to a five-membered ring and elimination of CO must take place. This process of CO elimination in phenol was observed by Horn et al.,[19] where, in addition to phenol, cyclopentadiene was the main product. We found out that CO elimination from the six-membered ring prior to ring contraction has a very high barrier (∼95 kcal/mol), whereas the overall barrier for the reaction *o*-hydroxybenzonitrile → cyclopentadienecarbonitrile + CO is some 20 kcal/mol lower when ring contraction occurs prior to CO elimination. We have thus decided to examine only the latter.

The first step on both surfaces is 1,3-H atom migration from oxygen O(9) to the nearest carbon atom in the benzene ring: to C(1) via transition state TS3a (Figure 5) and to C(3) via transition states TS3b (Figure 6). The migration to C(3) is preceded by a very fast rotation of the OH group toward C(3) with a barrier of ∼5 kcal/mol.

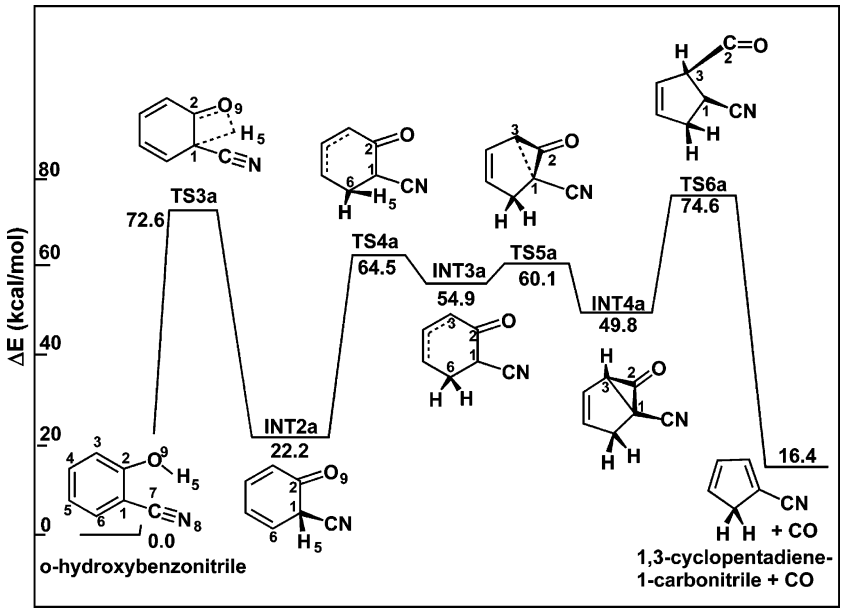


**Figure 5.** Reaction pathway of *o*-hydroxybenzonitrile decomposition to form 1,3-cyclopentadiene-1-carbonitrile. The first step is a H-atom shift from O(9) to C(1). Relative energies (in kcal/mol) are calculated at the uQCISD(T)//uB3LYP/cc-pVDZ level of theory.

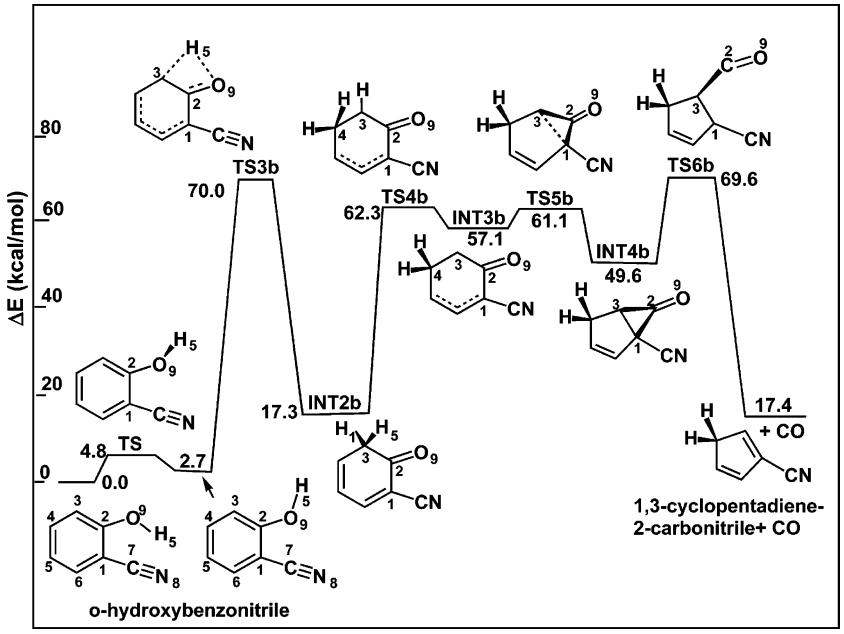


**Figure 6.** Reaction pathway of *o*-hydroxybenzonitrile decomposition to form 1,3-cyclopentadiene-2-carbonitrile. The first step is a H-atom shift from O(9) to C(3). Relative energies (in kcal/mol) are calculated at the uQCISD(T)//uB3LYP/cc-pVDZ level of theory.

**TABLE 3: Total Energies $E_{total}$ (in au), Zero Point Energies, Relative Energies $\Delta E$,[a] Imaginary Frequencies,[b] and Entropies[c] of the Species on the *o*-Hydroxybenzonitrile → Cyclopentadienecarbonitrile + CO Potential Energy Surface**

| | B3LYP | | | | | QCISD(T) | |
|---|---|---|---|---|---|---|---|
| species | $E_{total}$ | $\Delta E^a$ | ZPE | $S^c$ | $\nu^b$ | $E_{total}$ | $\Delta E^a$ |
| *o*-hydroxybenzonitrile | −399.742953 | 0.0 | 64.9 | 83.57 | | −398.655963 | 0.0 |
| Pathway 1 (Figure 5) | | | | | | | |
| TS3a | −399.620561 | 72.6 | 60.7 | 83.68 | (i − 2080) | −398.533505 | 72.6 |
| INT2a | −399.696777 | 27.9 | 63.8 | 86.40 | | −398.618762 | 22.2 |
| TS4a | −399.636574 | 63.1 | 61.2 | 84.43 | (i − 1012) | −398.547216 | 64.5 |
| INT3a | −399.650128 | 55.6 | 62.3 | 87.97 | | −398.564267 | 54.9 |
| TS5a | −399.636446 | 64.1 | 62.2 | 83.97 | (i − 257) | −398.555821 | 60.1 |
| INT4a | −399.648592 | 57.0 | 63.0 | 85.40 | | −398.573647 | 49.8 |
| TS6a | −399.612292 | 78.8 | 61.7 | 87.72 | (i − 478) | −398.532063 | 74.6 |
| 1,3-cyclopentadiene-1-carbonitrile + CO | −399.689121 | 29.2 | 60.4 | 123.58 | | −398.622599 | 16.4 |
| Pathway 2 (Figure 6) | | | | | | | |
| TS3b | −399.627968 | 67.7 | 60.5 | 83.46 | (i − 2088) | −398.537374 | 70.0 |
| INT2b | −399.707655 | 20.9 | 63.7 | 87.53 | | −398.626513 | 17.3 |
| TS4b | −399.639835 | 61.1 | 61.3 | 84.53 | (i − 795) | −398.550827 | 62.3 |
| INT3b | −399.645561 | 58.1 | 62.0 | 88.05 | | −398.560298 | 57.1 |
| TS5b | −399.634581 | 65.2 | 62.1 | 83.76 | (i − 216) | −398.554107 | 61.1 |
| INT4b | −399.649123 | 57.0 | 63.1 | 85.38 | | −398.574003 | 49.6 |
| TS6b | −399.620676 | 73.6 | 61.8 | 86.69 | (i − 446) | −398.540141 | 69.6 |
| 1,3-cyclopentadiene-2-carbonitrile + CO | −399.685932 | 31.0 | 60.2 | 123.68 | | −398.620671 | 17.4 |
| 1,3-Cyclopentadiene-2-carbonitrile ↔ 1,3-Cyclopentadiene-1-carbonitrile Isomerization | | | | | | | |
| 1,3-cyclopentadiene-2-carbonitrile | −286.364563 | 0.0 | 57.0 | 76.43 | | −285.565204 | 0.0 |
| TS7 | −286.324266 | 23.3 | 55.1 | 75.15 | (i − 1187) | −285.519225 | 26.9 |
| 1,3-cyclopentadiene-1-carbonitrile | −286.367752 | −1.8 | 57.2 | 76.33 | | −285.567132 | −1.0 |

[a] Relative energies in kcal/mol. $\Delta E = \Delta E_{total} + \Delta$(ZPE). [b] Imaginary frequency in $cm^{-1}$ [c] Entropies at 298 K in cal/(K mol).

The energy level of the transition states TS3a and TS3b are rather high, 72.6 kcal/mol for TS3a and 70.0 kcal/mol for TS3b. These high levels are due, to some extent, to the loss of resonance in the benzene ring. The intermediates INT2a and INT2b, on the other hand, are much more stable in view of the formation of new very strong C═O bonds. Their energy levels are only 22.2 kcal/mol for INT2a and 17.3 for INT2b above that of *o*-hydroxybenzonitrile.

The next step toward the ring contraction is an additional H-atom shift, that is, 1,2 H-atom shift from each one of the carbon atoms C(1) (Figure 5) and C(3) (Figure 6). These shifts will facilitate the formation of fused three- and five-membered rings toward the ring contraction. The transition states TS4a and TS4b are at relatively high energy level (64.5 and 62.3 kcal/mol, respectively). This is due to the fact that INT3a and INT3b are unstable. Their instability is caused by the transition from a $sp^2$ hybridization of the carbon atoms C(6) (Figure 5) and C(4) (Figure 6) to a $sp^3$ hybridization that destroys the three double bond conjugation that exists in INT2a and INT2b.

The transition states TS5a and TS5b that follow lead to the formation of fused three- and five-membered rings. These two rings are shown in the intermediates INT4a and INT4b that, via transition states TS6a and TS6b, produce 1,3-cyclopentadiene-1-carbonitrile + CO (Figure 6) and 1,3-cyclopentadiene-2-carbonitrile + CO (Figure 6). The formation of cyclopentadienecarbonitrile via transition states TS6a and TS6b involves

**TABLE 4: Several Structural Parameters of the Species Involved in the Reaction *o*-Hydroxybenzonitrile → 1,3-Cyclopentadiene-1-carbonitrile + CO Calculated at the B3LYP/cc-pVDZ Level of Theory**

| parameter [a,b] | *o*-hydroxy-benzonitrile | TS3a | INT2a | TS4a | INT3a | TS5a | INT5a | TS6a | 1,3-cyclopenta-diene-1-carbonitrile |
|---|---|---|---|---|---|---|---|---|---|
| C(1)−C(2) | 1.415 | 1.482 | 1.558 | 1.483 | 1.459 | 1.468 | 1.507 | 2.145 | − |
| C(2)−C(3) | 1.401 | 1.422 | 1.470 | 1.462 | 1.469 | 1.456 | 1.471 | 1.478 | − |
| C(3)−C(4) | 1.392 | 1.379 | 1.355 | 1.382 | 1.402 | 1.452 | 1.500 | 1.526 | 1.461 |
| C(4)−C(5) | 1.403 | 1.438 | 1.459 | 1.407 | 1.379 | 1.347 | 1.340 | 1.340 | 1.355 |
| C(5)−C(6) | 1.390 | 1.368 | 1.345 | 1.412 | 1.467 | 1.468 | 1.511 | 1.508 | 1.501 |
| C(6)−C(1) | 1.415 | 1.457 | 1.512 | 1.483 | 1.481 | 1.510 | 1.543 | 1.518 | 1.512 |
| C(6)−C(7) | 1.432 | 1.447 | 1.467 | 1.423 | 1.413 | 1.422 | 1.437 | 1.400 | 1.421 |
| C(7)−N(8) | 1.166 | 1.165 | 1.161 | 1.166 | 1.169 | 1.167 | 1.164 | 1.174 | 1.166 |
| C(2)−O(9) | 1.353 | 1.277 | 1.215 | 1.230 | 1.233 | 1.211 | 1.195 | 1.160 | − |
| O(9)−H(1) | 0.973 | 1.383 | 2.777 | − | − | − | − | − | − |
| C(1)−H(5) | 2.458 | 1.424 | 1.112 | 1.483 | − | − | − | − | − |
| C(6)−H(5) | − | − | 2.654 | 1.210 | 1.113 | − | − | − | − |
| C(1)−C(3) | − | − | 2.572 | 1.619 | 2.429 | 2.040 | 1.612 | 1.489 | 1.363 |

[a] Distances are in angstroms. [b] The atom numbering is shown in Figure 5.

**TABLE 5: Several Structural Parameters of the Species Involved in the Reaction *o*-Hydroxybenzonitrile → 1,3-Cyclopentadiene-2-carbonitrile + CO Calculated at the B3LYP/cc-pVDZ Level of Theory**

| parameter[a,b] | *o*-hydroxy-benzonitrile | TS3b | INT2b | TS4b | INT3b | TS5b | INT5b | TS6b | 1,3-cyclopenta-diene-2-carbonitrile |
|---|---|---|---|---|---|---|---|---|---|
| C(1)−C(2) | 1.413 | 1.432 | 1.490 | 1.474 | 1.483 | 1.474 | 1.437 | 2.074 | − |
| C(2)−C(3) | 1.401 | 1.455 | 1.529 | 1.459 | 1.439 | 1.448 | 1.466 | 1.465 | − |
| C(3)−C(4) | 1.395 | 1.431 | 1.495 | 1.398 | 1.463 | 1.491 | 1.532 | 1.545 | 1.501 |
| C(4)−C(5) | 1.400 | 1.382 | 1.349 | 1.434 | 1.470 | 1.495 | 1.513 | 1.523 | 1.505 |
| C(5)−C(6) | 1.393 | 1.421 | 1.450 | 1.388 | 1.370 | 1.345 | 1.340 | 1.357 | 1.350 |
| C(6)−C(1) | 1.407 | 1.397 | 1.366 | 1.407 | 1.421 | 1.464 | 1.505 | 1.455 | 1.478 |
| C(6)−C(7) | 1.434 | 1.429 | 1.433 | 1.429 | 1.425 | 1.427 | 1.437 | 1.403 | 1.430 |
| C(7)−N(8) | 1.164 | 1.165 | 1.164 | 1.166 | 1.167 | 1.166 | 1.164 | 1.172 | 1.165 |
| C(2)−O(9) | 1.355 | 1.280 | 1.216 | 1.234 | 1.236 | 1.213 | 1.194 | 1.157 | − |
| O(9)−H(1) | 0.970 | 1.406 | 2.676 | − | − | − | − | − | − |
| C(3)−H(5) | 2.456 | 1.411 | 1.107 | 1.598 | − | − | − | − | − |
| C(4)−H(5) | − | − | 2.569 | 1.183 | 1.115 | − | − | − | − |
| C(1)−C(3) | − | − | − | − | 2.419 | 2.082 | 1.608 | 1.513 | 1.360 |

[a] Distances are in angstroms. [b] The atom numbering is shown in Figure 6.

two steps that occur simultaneously: destruction of the three-membered ring and elimination of CO. Note that the C(2)−C(3) distance in both TS6a and TS6b are long, 1.478 and 1.465 Å, respectively.

The two isomers of cyclopentadienecarbonitrile that are produced from *o*-hydroxybenzonitrile interisomerize by H-atom shift only, without the involvement of the CN group. A similar process in other cyclopentadiene derivatives was observed in the past.[20−23] The barrier for the isomerization is only ∼28 kcal/mol, suggesting that the two isomers are at equilibrium at the very early stages of the *o*-hydroxybenzonitrile decomposition.

**3. Multiwell Calculations and Kinetic Modeling on the Potential Energy Surfaces.** To evaluate a global rate constant $k_f$ of a given process that is composed of several elementary steps, a kinetic scheme has to be constructed, containing all the elementary steps on the surface. To obtain a forward rate constant, both the forward and the back reactions of all the steps have to be included, except for the back reaction of the last step.

Two reaction schemes, one for the reaction benzoxazole → *o*-hydroxybenzonitrile and one for the reaction *o*-hydroxybenzonitrile → cyclopentadienecarbonitrile, have been constructed and are shown in Table 6. The rate constants of the elementary steps in the scheme were evaluated by the quantum chemical calculations at several temperatures as previously described, covering the temperature range at which the single pulse shock-tube experiments were carried out. These were then plotted as ln $k$ vs $1/T$ to obtain Arrhenius-type rate constants. Tunneling corrections were done only for steps 3 and 7 (Table 6), where the imaginary frequency of their transition states were higher than 1200 $cm^{-1}$ (Tables 1 and 3). These rate constants together with the calculated thermodynamic properties of the species involved (reactant and intermediates) were introduced into each one of the kinetic schemes, and computer modeling was performed. From the extent of the conversion to the products their production rate constant were calculated. The values obtained are

$$k(\text{benzoxazole} \rightarrow o\text{-hydroxybenzonitrile}) = 7.12 \times 10^{14} \exp(-63.5 \times 10^3/RT)\ s^{-1}$$

$$k(o\text{-hydroxybenzonitrile} \rightarrow \text{cyclopentadienecarbonitrile}) = 9.20 \times 10^{12} \exp(-67.8 \times 10^3/RT)\ s^{-1}$$

It is interesting to note that the reason for the higher pre-exponential factor of the first reaction by almost 2 orders of magnitude is that in the first reaction a ring is broken.

To compare the mole percents of the products obtained in the shock tube experiment and in the calculations, a reaction scheme for the system

$$\text{benzoxazole} \rightarrow o\text{-hydroxybenzonitrile} \quad (1)$$

$$o\text{-hydroxybenzonitrile} \rightarrow \text{cyclopentadienecarbonitrile} \quad (2)$$

was constructed using the two rate constants obtained and the thermodynamic properties of the three molecules involved, and

**TABLE 6: Arrhenius Parameters of the Elementary Steps on Benzoxazole → *o*-Hydroxybenzonitrile and *o*-Hydroxybenzonitrile → Cyclopentadienecarbonitrile Potential Energy Surfaces**

| | $A^a$ | $E_a^b$ |
|---|---|---|
| PES of Benzoxazole → *o*-Hydroxybenzonitrile (Figure 4) | | |
| 1. benzoxazole → *o*-hydroxyisobenzonitrile | $1.75 \times 10^{15}$ | 65.46 |
| 2. *o*-hydroxyisobenzonitrile → *o*-hydroxybenzonitrile | $2.15 \times 10^{13}$ | 32.49 |
| PES of *o*-Hydroxybenzonitrile → 1,3-Cyclopentadiene-1-carbonitrile +CO (Figure 5) | | |
| 3. *o*-hydroxybenzonitrile → INT2a | $7.99 \times 10^{12}$ | 69.68 |
| 4. INT2a → INT3a | $6.01 \times 10^{12}$ | 41.97 |
| 5. INT3a → INT4a | $2.39 \times 10^{12}$ | 5.44 |
| 6. INT4a → 1,3-cyclopentadiene-1-carbonitrile + CO | $5.63 \times 10^{13}$ | 25.79 |
| PES of *o*-Hydroxybenzonitrile → 1,3-Cyclopentadiene-2-carbonitrile +CO (Figure 6) | | |
| 7. *o*-hydroxybenzonitrile → INT2b | $3.81 \times 10^{13}$ | 71.66 |
| 8. INT2b → INT3b | $1.67 \times 10^{13}$ | 46.36 |
| 9. INT3b → INT4b | $1.90 \times 10^{12}$ | 4.80 |
| 10. INT4b → 1,3-cyclopentadiene-2-carbonitrile + CO | $5.08 \times 10^{13}$ | 21.16 |
| PES of 1,3-Cyclopentadiene-2-carbonitrile → 1,3-Cyclopentadiene-1-carbonitrile | | |
| 11. 1,3-cyclopentadiene-2-carbonitrile → 2,3-cyclopentadiene-1-carbonitrile | $2.80 \times 10^{13}$ | 27.84 |

[a] Pre-exponential factor in units of $s^{-1}$. [b] Activation energy in kcal/mol.

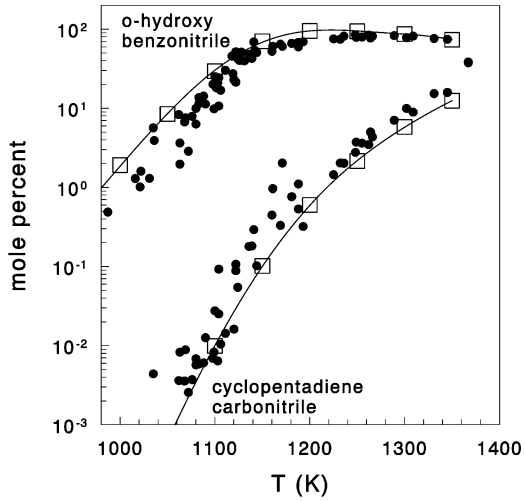


**Figure 7.** A comparison between the experimental and the calculated mole percents of *o*-hydroxybenzonitrile and cyclopentadienecarbonitrile. The experimental points (filled circles) are in very good agreement with the calculated points (open squares). The lines are the best fit to the calculated points.

computer modeling was performed. In this modeling the forward and the back reactions of the two processes were included. It should be mentioned that for the sake of comparison between the experimental data and the calculations, in both sets of data only the three compounds benzoxazole, *o*-hydroxybenzonitrile, and cyclopentadienecarbonitrile were considered. The obtained mole percent values of the two products are shown in Figure 7 in comparison with the experimental results. As can be seen, the agreement is excellent. Both the experimental and the calculated mole percent of cyclopentadiene-carbonitrile correspond to the sum of the mole percent of 1,3-cyclopentadiene-1-carbonitrile and 1,3-cyclopentadiene-2-carbonitrile, as these two isomers could not be separated in the GC analyses.

## V. Conclusions

(a) In view of the relative stability of benzoxazole, it decomposes at considerably higher temperature than both its isomers 2,1-bensisoxazole (anthranil) and 1,2-benisoxazole.

(b) The main products of benzoxazole decomposition are *o*-hydroxybenzonitrile and cyclopentadienecarbonitrile. Cyclopentadienecarbonitrile is not formed directly from benzoxazole but from its isomer *o*-hydroxybenzonitrile.

(c) A very good agreement between the experimental and the calculated data was obtained.

**Acknowledgment.** This research was supported by Grant # 34/01 from the Israel Science Foundation (ISF), Jerusalem, Israel.

## References and Notes

(1) Steele, W. V.; Chirico, R. D.; Knipmeyer, S. E.; Nguyen, A. *J. Chem. Thermodyn.* **1992**, *24*, 449.
(2) Matos, M. A.; Miranda M. S.; Morais, V. M. F.; Liebman, J. F. *Eur. J. Org. Chem.* **2004**, 3340.
(3) Lifshitz, A.; Tamburu, C.; Suslensky, A.; Dubnikova, F. *J. Phys. Chem. A*, part of the Chava Lifshitz memorial issue, in press.
(4) Lifshitz, A.; Laskin, A. *J. Chem. Phys.* **1997**, *101*, 7787.
(5) Westly, F.; Herron, J. T.; Cvetanovic, R. J.; Hampson, R. F.; Mallard, W. G. *NIST−Chemical Kinetics Standard Reference Database 17, Version5.0*, National Institute of Standards and Technology: Washington, DC.
(6) Becke, A. D. *J. Chem. Phys.* **1993**, *98*, 5648.
(7) Lee, C.; Yang, W.; Parr, R. G. *Phys. Rev.* **1988**, *B37*, 785.
(8) Dunning, T. H., Jr. *J. Chem. Phys.* **1989**, *90*, 107.
(9) Peng, C.; Schlegel, H. B. *Israel J. Chem.* **1993**, *33*, 449.
(10) Pople, J. A.; Head-Gordon, M.; Raghavachari, K. J. *J. Chem. Phys.* **1987**, *87*, 5968.
(11) Harvey, J. N.; Aschi, M.; Schwarz, H.; Koch, W. *Theor. Chem. Acc.* **1998**, *99*, 95.
(12) Frisch, M. J.; Trucks, G. W.; Schlegel, H. B.; Scuseria, G. E., Robb, M. A.; Cheeseman, J. R.; Zakrzewski, V. G.; Montgomery, J. A., Jr.; Stratmann, R. E.; Burant, J. C.; Dapprich, S.; Millam, J. M.; Daniels, A. D.; Kudin, K. N.; Strain, M. C.; Farkas, O.; Tomassi, J.; Barone, V.; Cossi, M.; Cammi, R.; Mennucci, B.; Pomelli, C.; Adamo, C.; Clifford, S.; Oshterski, J.; Petersson, G. A.; Ayala, P. Y.; Cui, Q.; Morokuma, K.; Malick, D. K.; Rabuck, A. D.; Rahavachari, K.; Foresman, J. B.; Cioslowski, J.; Orviz, J. V.; Baboul, A. G.; Stefanov, B. B.; Liu, G.; Liashenko, A.; Piskorz, P.; Komarini, I.; Gomperts, R.; Martin, R. L.; Fox, D. J.; Keith, T.; Al-Laham, M. A.; Peng, C. Y.; Nanayakkara, A.; Gonzalez, C.; Challacombe, M.; Gill, P. M. W.; Johnson, B.; Chen, M. W.; Wong, M. W.; Andres, J. L.; Head-Gordon, M.; Replogle, E. S.; Pople, J. A. *Gaussian 98, Revision A.7*; Gaussian, Inc., Pittsburgh, PA, 1998.
(13) Eyring, H. *J. Chem. Phys.* **1935**, *3*, 107.
(14) Evans, M. G.; Polanyi, M. *Trans. Faraday Soc.* **1935**, *31*, 875.
(15) Wigner, E. *Z. Phys. Chem.* **1932**, *B19*, 203.
(16) Louis, F.; Gonzales, C. A.; Huie, R.; Kurylo, M. J. *J. Phys. Chem. A* **2000**, *104*, 8773.
(17) George, P.; Glusker, J. P.; Bock, W. *J. Phys. Chem. A* **2000**, *104*, 11347.
(18) Dubnikova, F.; Lifshitz, A. *J. Phys. Chem. A* **2001**, *105*, 3605 and references therein.
(19) Horn, C.; Roy, K.; Frank, P.; Just, T. *Proc. Combust. Inst.* **1998**, *27*, 321.
(20) Roth, W. R. *Tetrahedron Lett.* **1964**, 1009.
(21) McLean, S.; Webster, C. J.; Rutherford, R. J. D. *Can. J. Chem.* **1969**, *47*, 1555.
(22) Bachrach, S. M. *J. Org. Chem.* **1993**, *58*, 5414.
(23) Dubnikova, F.; Lifshitz, A. *J. Phys. Chem. A* **2002**, *106*, 8173.